Inorganic Chemistry

Article

pubs.acs.org/IC

Tetranuclear Lanthanide Complexes Containing a Hydrazone-type Ligand. Dysprosium [2 × 2] Gridlike Single-Molecule Magnet and Toroic

Alexey Gusev,*[,†] Radovan Herchel,[‡] Ivan Nemec,[‡] Victor Shul'gin,[†] Igor L. Eremenko,[§] Kostantin Lyssenko,[∥] Wolfgang Linert,[⊥] and Zdeněk Trávníček*[,‡]

[†]General and Physical Chemistry Department, Crimean Federal University, Simferopol, Crimea

[‡]Department of Inorganic Chemistry, RCPTM, Faculty of Science, Palacký University, Olomouc, Czech Republic

[§]N. S. Kurnakov Institute of General and Inorganic Chemistry and [∥]A. N. Nesmeyanov Institute of Organoelement Compounds, Russian Academy of Sciences, Moscow, Russia

[⊥]Institute of Applied Synthetic Chemistry, Vienna University of Technology, Vienna, Austria

Supporting Information

ABSTRACT: A multidentate hydrazone-type ligand (*Z*,*Z*)-bis(1-(pyridin-2-yl)-1-amino-methylidene)oxalohydrazide (H_2L) was utilized in the synthesis of three new isomorphous tetranuclear complexes of the general formula $[Ln_4(HL)_4(H_2L)_2(NO_3)_4](NO_3)_4{\cdot}4CH_3OH$ (Ln = Gd^{III}, **1**, Tb^{III}, **2**, Dy^{III}, **3**) with the gridlike [2 × 2] topology. The analysis of the static magnetic data revealed weak antiferromagnetic interaction among lanthanide(III) atoms, whereas dynamic magnetic data led to the observation of the single-molecule magnet behavior in zero static magnetic field for the Dy_4 compound **3** with U_{eff} = 42.6 K and $\tau_0 = 1.50 \times 10^{-5}$ s. The theoretical CASSCF calculations supported also the presence of the net toroidal magnetic moment, which classifies compound **3** also as a single-molecule toroic.

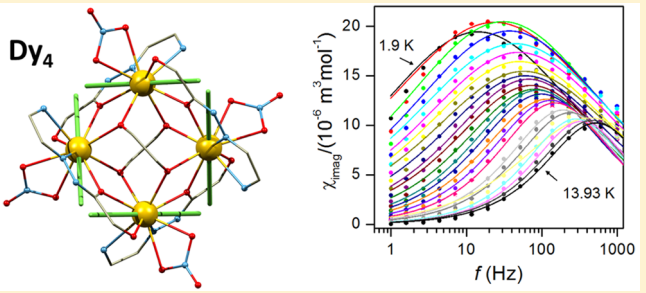

INTRODUCTION

The coordination compounds exhibiting slow relaxation of magnetization on molecular level, so-called single-molecule magnets (SMMs), attract a lot of attention due to their potential applications in high-density information storage, quantum computing, and molecular spintronics.[1] The magnetic bistability of these molecular nanomagnets is associated with the effective energy barrier (U) to reversal of the magnetization, and the key property, which defines the height of this barrier, is the uniaxial Ising-like magnetic anisotropy. It has been shown that lanthanides, especially Dy^{III}, Tb^{III}, and Er^{III}, are the most promising components for observing large U and high blocking temperature due to their large spin−orbit coupling and high magnetic moment.[2] Indeed, two novel Dy^{III} compounds published very recently established new records in blocking temperature (T = 20 K) and in the effective energy barrier (U_{eff} = 1025 K) in the class of SMMs.[3]

Furthermore, it has been shown on numerous examples during the past decade that a very promising strategy for obtaining high-barrier SMMs is a preparation of polynuclear Dy^{III} clusters.[4] Thus, a number of Dy-containing compounds exhibiting different topologies based on a dimeric, a triangular, a defect-dicubane, or a square-pyramidal core, or a wheel, has been described in the literature.[5] Among them, a tetranuclear Dy^{III} cluster with a [2 × 2] grid geometry showed the highest anisotropic barrier, U = 143 cm^{-1} (206 K), for the reported Dy_4 SMMs.[6] Furthermore, some polynuclear Dy^{III} compounds with Ising-like magnetic anisotropy and vortex distributions of magnetic dipoles not only exhibit SMM properties but also possess the toroidal magnetic moment.[7] This is regarded as the third kind of electromagnetic moment after the traditional polarization and magnetization, and such bistable molecules with a toroidal magnetic state were called single-molecule toroics (SMTs).[8] So far, there is only one example of a tetranuclear Dy^{III} complex, $[Dy_4(\mu_3\text{-}OH)_2(\mu\text{-}OH)_2(2,2\text{-bpt})_4(NO_3)_4(EtOH)_2]$ (2,2-bptH = 3,5-bis(pyridin-2-yl)-1,2,4-triazole), exhibiting such properties.[9]

In this article, we report on structural and magnetic properties of a new group of tetranuclear gridlike [2 × 2] Ln_4 complexes with the multidentate ligand (*Z*,*Z*)-bis(1-(pyridin-2-yl)-1-amino-methylidene)oxalohydrazide (H_2L; Scheme 1). The H_2L ligand was previously used in the synthesis of 3d metal complexes such as dinuclear $[Mn_2(H_2L)(NO_3)_2(CH_3OH)_2(H_2O)_2](NO_3)_2{\cdot}H_2O$, tetranuclear $[Fe_4(H_2L)_4](ClO_4)_6{\cdot}7.5H_2O$, $[Co_4(H_2L)_4]Br_6{\cdot}9H_2O$,

Received: October 10, 2016

DOI: 10.1021/acs.inorgchem.6b02449
Inorg. Chem. XXXX, XXX, XXX−XXX

Scheme 1. Pathway Showing the Preparation of the H_2L Ligand and the Reported Complexes 1−3

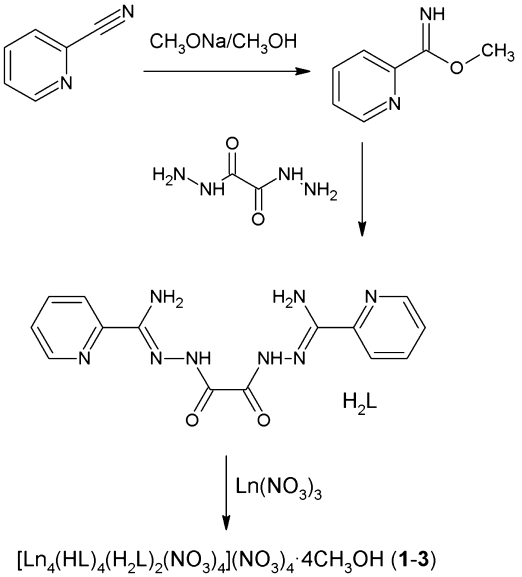

$[Co_4(HL)_4](NO_3)_6{\cdot}4CH_3OH{\cdot}CH_3CN{\cdot}9H_2O$, $[Ni_4(H_2L)_6](BF_4)_6F_2{\cdot}14H_2O$, or octanuclear $\{[Co_4(H_2L)_4]_2\}[Co(NCS)_4]_2(NCS)_4{\cdot}8CH3OH{\cdot}11H_2O$,[10] but it has not been used in lanthanide chemistry before. Herein, we report on the crystal structure and detailed experimental and theoretical investigations of magnetic properties of the selected lanthanide(III) complexes with the general formula $[Ln_4(HL)_4(H_2L)_2(NO_3)_4](NO_3)_4{\cdot}4CH_3OH$ (Ln = Gd^{III}, **1**, Tb^{III}, **2**, Dy^{III}, **3**).

EXPERIMENTAL SECTION

General Methods. Elemental analyses of C, H, and N were performed with a Perkin-Elmer 240 C analyzer. The X-ray powder diffraction patterns of all solid samples were recorded on a MiniFlex600 (Rigaku) instrument equipped with the Bragg−Brentano geometry, and with iron-filtered Cu $K\alpha_{1,2}$ radiation. Direct-current (DC) magnetic measurements were performed with MPMS XL7 SQUID magnetometer for **1** (T = 1.9−300 K at B = 0.1 T; B = 0−5 T at T = 2 and 5 K) and with a PPMS Dynacool VSM magnetometer for **2**−**3** (T = 1.9−300 K at B = 0.1 T; B = 0−9 T at T = 2, 5, and 10 K). The magnetic data were corrected for sample holder signal and for diamagnetic susceptibility. Measurements of alternating-current (AC) susceptibility were performed in a 3.8 Oe with AC field oscillating at various frequencies from 1 to 1500 Hz and with various DC fields using an MPMS XL7 SQUID magnetometer

X-ray Crystallography. X-ray diffraction experiments on the selected crystal of **1** were performed on a Bruker SMART APEX II automated diffractometer equipped with a CCD detector and a monochromatic radiation source (Mo Kα radiation, λ = 0.710 73 Å). The molecular structure was solved by direct methods using SHELX-2014,[11] and all the non-hydrogen atoms were refined anisotropically by SHELXS-2014.[11] All the hydrogen atoms were found in differential Fourier maps, and their parameters were refined using a riding model with U_{iso}(H) = 1.2 (CH, CH_2, NH_2, NH) or 1.5 (CH_3) U_{eq}. Nonroutine aspects of structure refinement: The electron density from heavily disordered methanol molecules was removed by SQUEEZE procedure.[12]

Synthesis. *Preparation of H_2L.* Sodium metal (0.8 g) was added carefully to 35 cm^3 of methanol followed by addition of 2-pyridine carbonitrile (10.9 g, 104 mmol). The solution rested for 30 min. Then, oxalic dihydrazide (4.8 g, 0.040 mol) was added, and refluxing of mixture for 10 h resulted in precipitation of a yellow powder. The mixture was cooled to room temperature, and the product was filtered off, washed with water, methanol, and diethyl ether, and dried in vacuum. (found: C, 51.71; H, 4.17; N, 34.04%. $C_{14}H_{14}N_8O_2$ requires C, 51.53; H, 4.31; N, 34.33%).

General Procedure for the Preparation of Complexes. $Ln(NO_3)_3{\cdot}nH_2O$ (Ln−Dy^{III}, Gd^{III} and Tb^{III} (1.0 mmol) in methanol (10 cm^3) was added to a hot suspension of H_2L (0.46 g, 1.5 mmol) in methanol (10 cm^3). The mixture was stirred while heated. The obtained yellow solution was filtered and allowed to stand at room temperature. Yellow crystals, suitable for structural analysis formed during the next day (yield 37−53%).

$[Dy_4(HL)_4(H_2L)_2(NO_3)_4](NO_3)_4{\cdot}4MeOH$. Found C 32.71; H 3.12; N 24.19%. $C_{88}H_{96}N_{56}O_{40}Dy_4$ requires: C 32.74; H 2.99; N 24.29.

$[Tb_4(HL)_4(H_2L)_2(NO_3)_4](NO_3)_4{\cdot}4MeOH$. Found C 32.06; H 2.73; N 24.92%. $C_{88}H_{96}N_{56}O_{40}Tb_4$ requires: C 32.89; H 3.01; N 24.41

$[Gd_4(HL)_4(H_2L)_2(NO_3)_4](NO_3)_4{\cdot}4MeOH$. Found C 32.26; H 3.08; N 24.63%. $C_{88}H_{96}N_{56}O_{40}Gd_4$ requires: C 32.96; H 3.02; N 24.46

Theoretical Calculations. The post-Hartree−Fock calculations for the mononuclear $[Dy(HL)_2(H_2L)_2(NO_3)]$ fragment of **3** (Figure S6) based on the experimental X-ray structure were performed with the MOLCAS 8.0 program package.[13] The active space of the CASSCF calculations[14] comprised of nine electrons in seven metal-based f-orbitals (CAS(9,7). All 21 sextet, 224 quartet, and 490 doublet states were considered in the CASSCF calculations by employing the RASSCF method. The spin−orbit coupling based on atomic mean field approximation (AMFI)[15] was taken into account using RASSI-SO

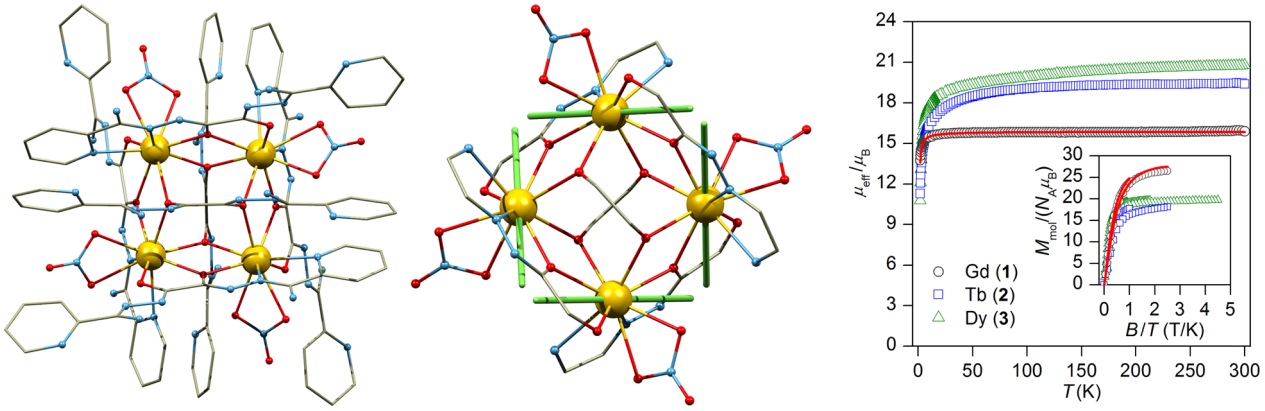

Figure 1. Molecular structure of the $[Ln_4(HL)_4(H_2L)_2(NO_3)_4]^{4+}$ complex cation of **3** with the omitted hydrogen atoms (left) (CCDC 1483169). The detailed view on the core of **3** with ab initio computed orientation of the principal magnetization axes of the ground-state Kramers doublets (middle). Static magnetic data for **1**−**3** (right). The lines represent the calculated data for **1** using eq 1, with the values of J = −0.013 cm^{-1}, D = −0.21 cm^{-1}, g = 1.997.

DOI: 10.1021/acs.inorgchem.6b02449
Inorg. Chem. XXXX, XXX, XXX−XXX

with 21 sextet, 128 quartet, and 130 doublet states. The relativistic effects were treated with a Douglas−Kroll Hamiltonian.[16] The following basis sets were employed: Dy.ANO-RCC-VQZP for Dy atom, O.ANO-RCC-VTZP for oxygen atoms directly bounded to Dy atom, O.ANO-RCC-MB for other oxygen atoms, N.ANO-RCC-VTZP for nitrogen atoms directly bounded to Dy atom, N.ANO-RCC-MB for other nitrogen atoms, C.ANO-RCC-MB for carbon atoms, and H.ANO-RCC-MB for hydrogen atoms.[17] The resulting wave functions and the energies of the molecular multiplets were used for the calculation of the magnetic properties, g tensors of the lowest Kramers doublet states, and blocking barrier using module SINGLE_ANISO (Figures 1, 3, and S6 and Table 1).[18] Afterward, the module POLY_ANISO was utilized to calculate magnetic properties and energy levels for whole Dy_4 complex $[Dy_4(HL)_4(H_2L)_2(NO_3)_4]^{4+}$ of **3** employing S_4 symmetry (Figures 4, 5, and S8).[19,7g]

Table 1. Energy Levels of Lowest Ligand Field Multiplets in Zero Magnetic Field Derived from CASSCF/DKH2/SINGLE_ANISO Calculations for the Molecular Fragment $[Dy(HL)_2(H_2L)_2(NO_3)]$ of Complex 3 with the Respective g-Factors Derived for Each Kramers Doublet with Effective Spin 1/2

energy (K)	g_x	g_y	g_z	α^a (deg)
0.0	0.005	0.007	19.86	
307	0.26	0.45	17.82	32.3
386	0.45	1.28	13.77	30.5
482	4.97	6.06	9.38	28.2
589	0.38	3.64	10.62	66.6
653	1.36	3.72	14.29	78.7
730	0.37	0.64	16.46	73.9
801	0.29	1.01	18.10	94.4

[a] α is an angle of g_z of the excited state with respect to g_z of ground Kramers doublet.

The density functional theory (DFT) calculations were performed with the program ORCA 3.0.[20] The hybrid B3LYP functional[21] was used for the calculations of the isotropic exchange constants J following Ruiz's approach[22] by comparing the energies of high-spin (HS) and broken-symmetry (BS) spin states. The relativistic effects were also included in the calculation with zero-order regular approximation (ZORA)[23,24] together with the scalar relativistic contracted version of the basis functions: def2-TZVP for gadolinium atoms, def2-TZVP(-f) for nitrogen and oxygen atoms, and def2-SVP for carbon and hydrogen atoms.[25]

The calculations utilized the RI approximation with the decontracted auxiliary def2-TZVP/J, def2-TZV/J, and def2-SVP/J Coulomb fitting basis sets and the chain-of-spheres (RIJCOSX) approximation to exact exchange as implemented in ORCA.[26] Increased integration grids (Grid5 in ORCA convention) and tight self-consistent field convergence criteria were used in all the calculations. The isotropic exchange parameter J for the spin Hamiltonian used in eq 1 was calculated for $[Gd_4(HL)_4(H_2L)_2(NO_3)_4]^{4+}$ molecular fragment, which was extracted from experimental X-ray data of **3** by replacing Dy atoms with Gd atoms. Then, the relationship $J = (E_{BS13} - E_{HS})/224$ was used to quantify J as -0.0191 cm^{-1}.

RESULTS AND DISCUSSION

Syntheses and General Characterization. The polydentate ligand H_2L shown in Scheme 1 reveals the potential to bind to metals in a variety of different ways, with involvement of 2-pyridyl moieties and/or the oxalylhydrazone ones. Except for that, the ligand nominally has two ionizable protons, and their role is to provide not only a scaffold for metal ion coordination but also an overall charge balance.

The reaction conditions needed to produce specifically the Ln^{III} clusters **1**−**3** were optimized using a trial-and-error method, by changing the molar ratio of the reactants and solvents. It has been found that the variation of components ratio does not affect the composition of the resulting products indicating thus on self-assembly character of the reaction. In all the cases, the prepared complexes possess 2:3 Ln/H_2L molar ratio. The best yields for compounds **1**−**3** were obtained based on the reaction of $Ln(NO_3)_3{\cdot}nH_2O$ with H_2L in methanol, and the compounds were obtained as yellow crystals. The X-ray powder studies (Figure S1) of **1**−**3** demonstrate that all the complexes belong to an isostructural/isomorphous series.

Crystal Structure. The crystal structure of **3**, as the representative example of whole isostructural series, was determined by a single-crystal X-ray analysis (Table S1). The structure of the heteroleptic self-assembled Dy_4 [2 × 2] grid is shown in Figure 1. Each dysprosium atom is nine-coordinated (with the coordination geometry close to spherical capped square antiprism[27]) by one H_2L (η^3, tridentate chelate pocket involving 2-pyridyl and amidrazone nitrogen atoms, with the N_2O donor set) ligand, by one HL^- (η^2, bidentate chelate pocket, O_2) ligand, and by the nitrato ligand (η^2). One H_2L ligand is coordinated to the central atom by an oxygen atom in a monodentate manner and provides bridging (μ-O) between neighboring Dy atoms (Figure 1). Furthermore, this arrangement provides intramolecular stabilization of the molecule by two N−H···O hydrogen bonds (d(N···O) = 3.075(2) Å) between the amine groups located on the H_2L ligand and oxygen atoms from the coordinated nitrato ligands. The Dy−O bond lengths fall within the 2.329(7)−2.436(7) Å (for oxygen atoms from the H_2L and HL^- ligands) and 2.498(10)−2.523(8) Å ranges (for the coordinated nitrato ligand). Two Dy−N bonds adopt lengths as follows: 2.427(10) and 2.517(11) Å (Table S2). The arrangement of four Dy atoms is almost planar (average deviation of these atoms from the best-fit mean plane through the Dy_4 atoms is 0.008(2) Å. The intramolecular Dy···Dy distances, going through covalent bonding, are rather short (3.978 (3) Å).

Magnetic Properties. The static magnetic properties were measured for all the compounds as temperature dependence (1.9−300 K) of susceptibility and field dependence (0−7/9 T) of magnetization (Figure 1, right). From the obtained results it can be apparent that the room-temperature values of effective magnetic moment (μ_{eff}/μ_B) are in a good agreement with the expected values (the calculated values are in the parentheses): **1**, 15.9 (15.9); **2**, 19.4 (19.4); 20.8 (21.3). At low temperatures (below 100 K μ_{eff}/μ_B) the decrease in μ_{eff}/μ_B value is observed, and it is much more visible for **2** and **3** than for **1** due to depopulation of Stark levels arising from the ground state ($^7F_6$ in **2** and $^6H_{15/2}$ in **3**). In **1**, the small decrease in μ_{eff}/μ_B below 30 K can be ascribed to a weak antiferromagnetic interaction between the Gd^{III} atoms and small single-ion anisotropy. Both temperature- and field-dependent magnetic data were then simultaneously analyzed utilizing the following spin Hamiltonian

$$\hat{H} = -J\left(\sum_{i=1}^{3} \vec{S}_i{\cdot}\vec{S}_{i+1} + \vec{S}_1{\cdot}\vec{S}_4\right) + D\sum_{i=1}^{4} \hat{S}_{i,z}{}^2 - \hat{S}_i{}^2/3 + \mu_B B g_i \hat{S}_{i,a} \quad (1)$$

which resulted in these parameters: $J = -0.013$ cm^{-1}, $D = -0.21$ cm^{-1}, $g = 1.997$ (Figure 1). The fitted J-value is also in

DOI: 10.1021/acs.inorgchem.6b02449
Inorg. Chem. XXXX, XXX, XXX−XXX

good agreement with the calculated one $J = -0.019$ cm^{-1}, as supported by DFT calculations (see Experimental Section for details).

The dynamic magnetic data were acquired for compounds **2** and **3**. In the case of Tb^{III} complex **2**, the nonzero out-of-phase susceptibility was detected at nonzero static magnetic field, but the maxima were not observed until 1.9 K (Figures S2 and S3). Therefore, AC susceptibility data were analyzed with the simplified model[28] based on eq 2

$$\ln(\chi''/\chi') = \ln(2\pi f\tau_0) + U/kT \quad (2)$$

where higher-temperature AC data for higher applied frequencies (f) were analyzed as visualized in Figure S4, which resulted in $U = 9.2-13.2$ K. However, Dy^{III} complex **3** behaves as a single-molecule magnet (SMM) already at zero static field, and the temperature-dependent experimental data

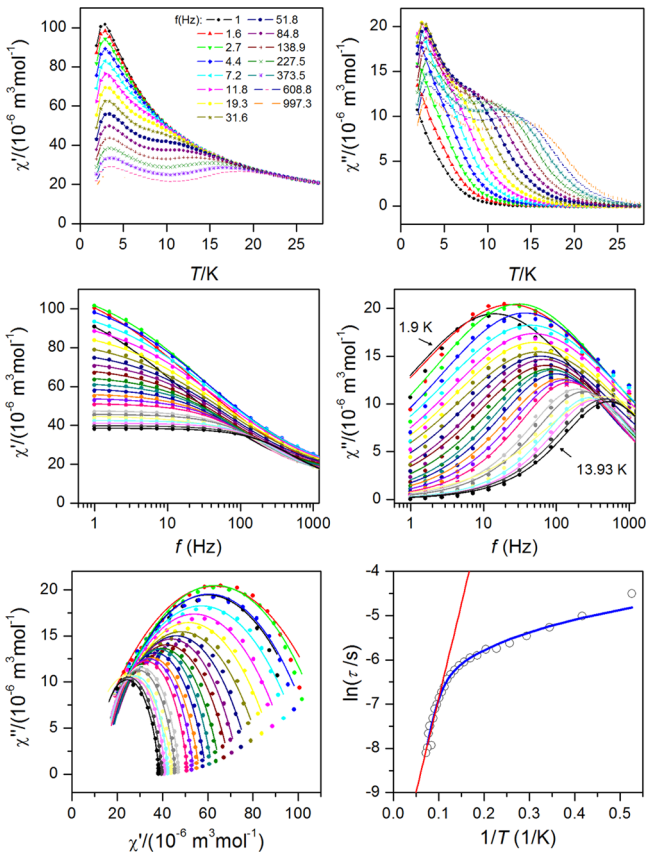

Figure 2. AC susceptibility data for Dy^{III} complex **3** at the zero applied external field $B_{DC} = 0.0$ T. (top) In-phase χ' and out-of-phase χ'' molar susceptibilities. Lines serve as guides for the eyes. (middle) Frequency dependence of χ' and χ'' molar susceptibilities. Full points—experimental data, full lines—fitted data using eq 3. (bottom) Argand (Cole−Cole) plot and fit of resulting relaxation times to Arrhenius law (red line) or to combination of Orbach and Raman relaxation processes (blue line).

(Figure 2) were possible to analyze with the one-component Debye model ($\omega = 2\pi f$)

$$\chi(\omega) = \chi_S + (\chi_T - \chi_S)/[1 + (i\omega\tau)^{1-\alpha}] \quad (3)$$

providing values of isothermal (χ_T) and adiabatic (χ_S) susceptibilities, relaxation times (τ), and distribution parameters (α)—Figure 2 and Table S3. This enabled us to construct the Argand (Cole−Cole) plot and subsequently to estimate reversal barrier $U = 42.6$ K with $\tau_0 = 1.50 \times 10^{-5}$ s (Figure 2) using Arrhenius law. Alternatively, $1/\tau = CT^n + 1/\tau_0 \cdot \exp(-U/kT)$ was used incorporating also Raman relaxation process, which resulted in $U = 67.6$ K, $\tau_0 = 3.53 \times 10^{-6}$ s, $C = 64.9$, and $n = 1.0$. Such obtained U is comparable to other tetranuclear gridlike Dy^{III} SMMs (see Table S4). Nonetheless, it must be stressed here that U reflects thermally activated Orbach relaxation mechanism, and thus it limits the analysis of AC susceptibility data only to the data having maxima in the Argand diagram. That means that data measured between $T = 1.9$ and 13.93 K could be the source of underestimation of U, because nonzero out-of-phase AC susceptibility signal is already observed below 28 K. Thus, AC susceptibility data were also analyzed with simplified model using eq 2, which resulted in much higher magnetic moment reversal barrier, $U = 217-270$ K, and $\tau_0 = 0.63-8.86 \times 10^{-10}$ s (Figure S5).

Theoretical Calculations. Ab initio CASSCF calculations with MOLCAS 8.0 for the mononuclear [Dy(HL)$_2$(H$_2$L)$_2$(NO$_3$)] fragment of **3** and subsequent analysis with Single_Aniso module revealed that $^6H_{15/2}$ atomic term is split into eight Kramers doublets (KD) (Figure 3 and Table 1).

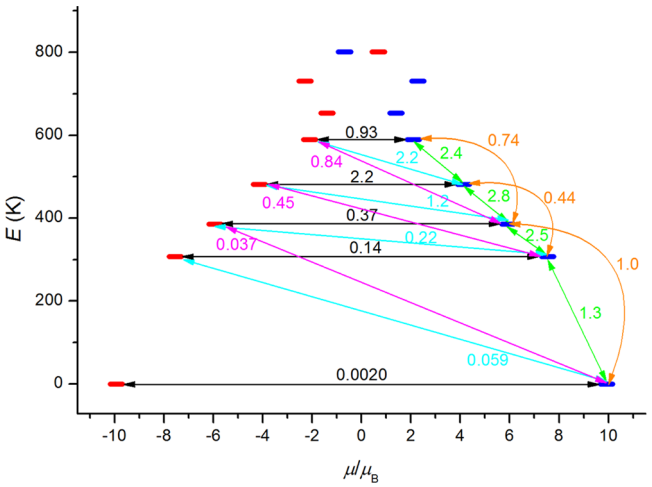

Figure 3. Ab initio computed magnetization blocking barrier for mononuclear moiety of **3**. The thick blue/red bars indicate the Kramer's doublets as a function of magnetic moment. Green/orange lines indicate the magnetization reversal mechanism. The cyan/magenta lines show the possible pathway of the Orbach process. The black lines represent the presence of QTM/TA-QTM between the connecting pairs. The numbers provided on each arrow are the mean absolute values for the corresponding matrix elements of the transition magnetic moment, and for values larger than 0.1 an efficient relaxation mechanism is expected.[29]

Each Kramers doublet was then analyzed with effective spin $S_{eff} = 1/2$, which resulted in effective g-tensor values (g_x, g_y, g_z). It is evident that ground state possesses a very large axial magnetic anisotropy, $g_x = g_y \approx 0$ and $g_z = 19.86$ (Table 1). The first and second excited states have also quite large axial magnetic anisotropy (Table 1), but g_x and g_y components are already nonzero and also we must note that easy axis of g-tensor of the ground state is not perfectly collinear with the easy axes of g-tensors of first and second excited states as visualized in Figure S6. This is also reflected in Figure 3, where the values of the transition magnetic moments between Kramers levels are

DOI: 10.1021/acs.inorgchem.6b02449
Inorg. Chem. XXXX, XXX, XXX−XXX

shown and this plot suggests that there is very low probability of the quantum tunneling of the ground state and that the relaxation through first excited states is most probable. This is also in agreement with the experiment, where analysis of AC susceptibility data resulted in the estimation of U_{eff} = 217−270 K (eq 2), which matches with the first excited state energy separation value ΔE = 307 K. All these facts support the observed zero-field SMM behavior of **3** and the relaxation pathway through the first excited state.

Subsequently, the experimental DC magnetic data were analyzed with the Poly_Aniso program utilizing S_4 symmetry of the molecule. Because of mutual orientation of the easy axes of all Dy atoms in Dy_4 unit as shown in Figure 1, there are important antiferromagnetic interactions mostly of dipolar origin between the magnetic dipoles of the respective Dy atoms. However, also additional antiferromagnetic coupling J_{ex} = −0.03 cm^{-1} was applied to obtain even better agreement with the experimental data—Figure 4. The impact of dipolar and exchange interactions is demonstrated in Figure 4. Evidently, the dipolar interactions are the main reason for the decrease of the effective magnetic moment at low temperature (Figure 4). Next outcome of these antiferromagnetic interactions within the tetramer unit is that there is a net toroidal magnetic moment in **3** (Figure 1), which means that this compound belongs to the class of the single-molecule toroics.[6] As a result, there is a nonmagnetic ground state, where the crossing from nonmagnetic to magnetic state is indicated at ∼0.5 T from CASSCF calculations as plotted in Figure 5. This is also manifested in the experimental maxima of χ_{mol} versus T found at T = 2.57 K (Figure 4) and of dM_{mol}/dB versus B found at B = 0.43 T (Figure S7). These characteristics were also recovered from theoretical calculations using Poly_Aniso module (Figure S8).

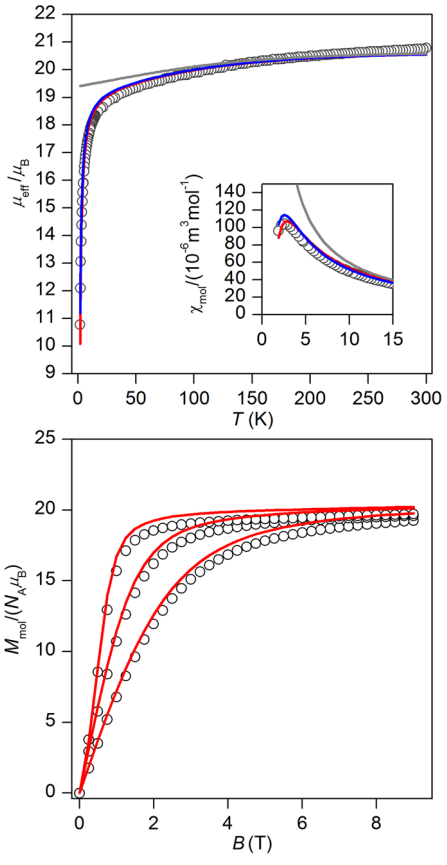

Figure 4. Magnetic data for **3**. (top) Temperature dependence of the effective magnetic moment and molar susceptibility measured at B = 0.1 T. (bottom) Isothermal magnetizations measured at T = 2, 5, and 10 K. Empty circles: experimental data. Full lines: calculated data using module POLY_ANISO scaled with the factor equal to 0.953. Gray line—calculation without any interactions, blue line—calculation with all the possible dipolar interactions, red line—calculation with all the possible dipolar interactions and additional exchange interactions J_{12} = J_{23} = J_{34} = J_{14} = −0.03 cm^{-1} applied.

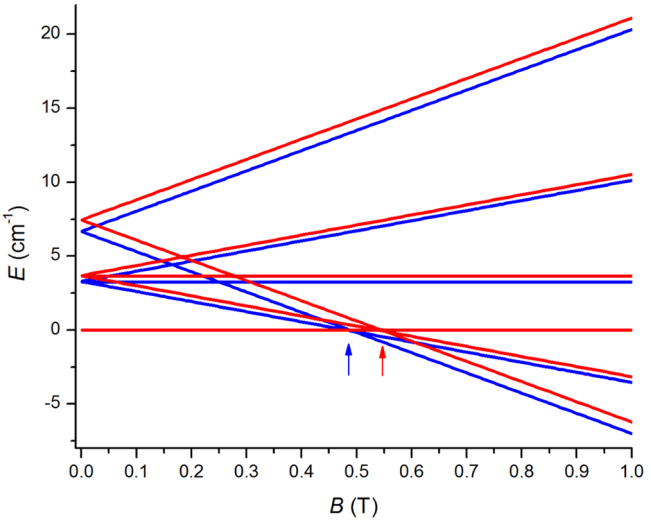

Figure 5. Course of the exchange states with magnetic field perpendicular to the plane of four Dy atoms of **3**. The blue and red lines correspond to dipolar and to dipolar + exchange coupling, respectively, accompanied by energy crossing from nonmagnetic to magnetic ground state indicated by blue and red arrows.

CONCLUSION

In conclusion, three novel tetranuclear 2 × 2 grid lanthanide complexes $[Ln_4(HL)_4(H_2L)_2(NO_3)_4](NO_3)_4{\cdot}4CH_3OH$ (Ln = Gd^{III}, **1**, Tb^{III}, **2**, Dy^{III}, **3**) were prepared, and their magnetism was thoroughly studied. In the case of the Gd^{III} compound **1**, the spin Hamiltonian formalism is valid, and weak antiferromagnetic exchange and relatively small magnetic anisotropy were found (J = −0.013 cm^{-1} and D = −0.21 cm^{-1}). The Tb^{III} compound **2** was found to behave as a field-induced SMM with the estimated U = 9.2−13.2 K. From the magnetic point of view, the most exciting is the Dy^{III} compound **3**, which behaves as zero-field SMM and net toroidal SMT. The effective barrier was estimated as U = 42.6 K up to U = 217−270 K depending on the applied procedure. The CASSCF calculations, followed by utilization of Single_Aniso and Poly_Aniso modules, were crucial for the proper understanding of the magnetic properties of this compound, both static and dynamic. Therefore, the compound **3** enlarges a small class of single-molecule magnets with net toroidal magnetic moment.

ASSOCIATED CONTENT

Supporting Information

The Supporting Information is available free of charge on the ACS Publications website at DOI: 10.1021/acs.inorgchem.6b02449.

DOI: 10.1021/acs.inorgchem.6b02449
Inorg. Chem. XXXX, XXX, XXX−XXX

Experimental details, figures and tables referring to syntheses, X-ray analysis, magnetic data analysis, and theoretical calculations (PDF)

AUTHOR INFORMATION

Corresponding Authors

*E-mail: galex0330@gmail.com. (A.G.)
*E-mail: zdenek.travnicek@upol.cz. (Z.T.)

ORCID

Radovan Herchel: 0000-0001-8262-4666

Notes

The authors declare no competing financial interest.

ACKNOWLEDGMENTS

We acknowledge the financial support from the following projects: LO1305 (C.Z.) and No. 3874 (R.U.). We also thank Dr. L. Ungur for fruitful discussions.

REFERENCES

(1) (a) Gatteschi, D.; Sessoli, R.; Villain, J. *Molecular Nanomagnets;* Oxford University Press: Oxford, U.K., 2006. (b) *Molecular Magnets Physics and Applications;* Bartolomé, J., Luis, F., Fernández, J. F., Eds.; Springer-Verlag: Berlin, Germany, 2014.

(2) (a) *Lanthanides and Actinides in Molecular Magnetism;* Layfield, R. A., Murugesu, M., Eds.; Wiley-VCH: Weinheim, Germany, 2015. (b) Woodruff, D. N.; Winpenny, R. E. P.; Layfield, R. A. Lanthanide Single-Molecule Magnets. *Chem. Rev.* **2013**, *113*, 5110−5148.

(3) (a) Chen, Y.-C.; Liu, J.-L.; Ungur, L.; Liu, J.; Li, Q.-W.; Wang, L.-F.; Ni, Z.-P.; Chibotaru, L. F.; Chen, X.-M.; Tong, M.-L. Symmetry-Supported Magnetic Blocking at 20 K in Pentagonal Bipyramidal Dy(III) Single-Ion Magnets. *J. Am. Chem. Soc.* **2016**, *138*, 2829−2837. (b) Liu, J.; Chen, Y.-C.; Liu, J.-L.; Vieru, V.; Ungur, L.; Jia, J.-H.; Chibotaru, L. F.; Lan, Y.; Wernsdorfer, W.; Gao, S.; Chen, X.-M.; Tong, M.-L. A Stable Pentagonal Bipyramidal Dy(III) Single-Ion Magnet with a Record Magnetization Reversal Barrier over 1000 K. *J. Am. Chem. Soc.* **2016**, *138*, 5441−5450.

(4) Tang, J.; Zhang, P. *Lanthanide Single Molecule Magnets;* Springer-Verlag: Berlin, Germany, 2015.

(5) (a) Gamer, M. T.; Lan, Y. H.; Roesky, P. W.; Powell, A. K.; Clerac, R. Pentanuclear Dysprosium Hydroxy Cluster Showing Single-Molecule-Magnet Behavior. *Inorg. Chem.* **2008**, *47*, 6581. (b) Hewitt, I.; Lan, Y. H.; Anson, C. E.; Luzon, J.; Sessoli, R.; Powell, A. K. Opening up a dysprosium triangle by ligand oximation. *Chem. Commun.* **2009**, 6765. (c) Layfield, R. A.; McDouall, J. J. W.; Sulway, S. A.; Tuna, F.; Collison, D.; Winpenny, R. E. P. Influence of the N-Bridging Ligand on Magnetic Relaxation in an Organometallic Dysprosium Single-Molecule Magnet. *Chem. - Eur. J.* **2010**, *16*, 4442. (d) Westin, L. G.; Kritikos, M.; Caneschi, A. Self assembly, structure and properties of the decanuclear lanthanide ring complex, Dy10-(OC2H4OCH3)30. *Chem. Commun.* **2003**, 1012. (e) Guo, Y.-N.; Xu, G.-F.; Gamez, P.; Zhao, L.; Lin, S.-Y.; Deng, R.; Tang, J.; Zhang, H.-J. Two-Step Relaxation in a Linear Tetranuclear Dysprosium(III) Aggregate Showing Single-Molecule Magnet Behavior. *J. Am. Chem. Soc.* **2010**, *132*, 8538. (f) Anwar, M. U.; Thompson, L. K.; Dawe, L. N.; Habib, F.; Murugesu, M. Predictable self-assembled [2 × 2] Ln(III)4 square grids (Ln = Dy,Tb)—SMM behaviour in a new lanthanide cluster motif. *Chem. Commun.* **2012**, *48*, 4576−4578. (g) Woodruff, D. N.; Tuna, F.; Bodensteiner, M.; Winpenny, R. E. P.; Layfield, R. A. Single-Molecule Magnetism in Tetrametallic Terbium and Dysprosium Thiolate Cages. *Organometallics* **2013**, *32*, 1224−1229. (h) Pugh, T.; Chilton, N. F.; Layfield, R. A. A Low-Symmetry Dysprosium Metallocene Single-Molecule Magnet with a High Anisotropy Barrier. *Angew. Chem., Int. Ed.* **2016**, *55*, 11082−11085. (i) Pugh, T.; Vieru, V.; Chibotaru, L. F.; Layfield, R. A. Magneto-structural correlations in arsenic- and selenium-ligated dysprosium single-molecule magnets. *Chem. Sci.* **2016**, *7*, 2128−2137.

(6) Guo, P.-H.; Liu, J.; Wu, Z.-H.; Yan, H.; Chen, Y.-C.; Jia, J.-H.; Tong, M.-L. Single-Molecule-Magnet Behavior in a [2 × 2] Grid $Dy^{III}4$ Cluster and a Dysprosium-Doped $Y^{III}4$ Cluster. *Inorg. Chem.* **2015**, *54*, 8087−8092.

(7) See, for example: (a) Das, C.; Vaidya, S.; Gupta, T.; Frost, J. M.; Righi, M.; Brechin, E. K.; Affronte, M.; Rajaraman, G.; Shanmugam, M. Single-Molecule Magnetism, Enhanced Magnetocaloric Effect, and Toroidal Magnetic Moments in a Family of Ln4 Squares. *Chem. - Eur. J.* **2015**, *21*, 15639−15650. (b) Xue, S. F.; Chen, X. H.; Zhao, L.; Guo, Y. N.; Tang, J. K. Two Bulky-Decorated Triangular Dysprosium Aggregates Conserving Vortex-Spin Structure. *Inorg. Chem.* **2012**, *51*, 13264−13270. (c) Wang, Y. X.; Shi, W.; Li, H.; Song, Y.; Fang, L.; Lan, Y. H.; Powell, A. K.; Wernsdorfer, W.; Ungur, L.; Chibotaru, L. F.; Shen, M. R.; Cheng, P. A single-molecule magnet assembly exhibiting a dielectric transition at 470 K. *Chem. Sci.* **2012**, *3*, 3366−3370. (d) Ungur, L.; Langley, S. K.; Hooper, T. N.; Moubaraki, B.; Brechin, E. K.; Murray, K. S.; Chibotaru, L. F. Net Toroidal Magnetic Moment in the Ground State of a {Dy6}-Triethanolamine Ring. *J. Am. Chem. Soc.* **2012**, *134*, 18554−18557. (e) Lin, S. Y.; Wernsdorfer, W.; Ungur, L.; Powell, A. K.; Guo, Y. N.; Tang, J. K.; Zhao, L.; Chibotaru, L. F.; Zhang, H. J. Coupling Dy3 Triangles to Maximize the Toroidal Moment. *Angew. Chem., Int. Ed.* **2012**, *51*, 12767−12771. (f) Hewitt, I. J.; Tang, J.; Madhu, N. T.; Anson, C. E.; Lan, Y.; Luzon, J.; Etienne, M.; Sessoli, R.; Powell. Coupling Dy3 Triangles Enhances Their Slow Magnetic Relaxation A. K. *Angew. Chem., Int. Ed.* **2010**, *49*, 6352−6356. (g) Ungur, L.; Van den Heuvel, W.; Chibotaru, L. F. Ab initio investigation of the non-collinear magnetic structure and the lowest magnetic excitations in dysprosium triangles. *New J. Chem.* **2009**, *33*, 1224−1230. (h) Luzon, J.; Bernot, K.; Hewitt, I. J.; Anson, C. E.; Powell, A. K.; Sessoli, R. Spin Chirality in a Molecular Dysprosium Triangle: The Archetype of the Noncollinear Ising Model. *Phys. Rev. Lett.* **2008**, *100*, 247205. (i) Chibotaru, L. F.; Ungur, L.; Soncini, A. The Origin of Nonmagnetic Kramers Doublets in the Ground State of Dysprosium Triangles: Evidence for a Toroidal Magnetic Moment. *Angew. Chem., Int. Ed.* **2008**, *47*, 4126−4129.

(8) Ungur, L.; Lin, S.-Y.; Tang, J.; Chibotaru, L. F. Single-molecule toroics in Ising-type lanthanide molecular clusters. *Chem. Soc. Rev.* **2014**, *43*, 6894−6905.

(9) Guo, P.-H.; Liu, J.-L.; Zhang, Z.-M.; Ungur, L.; Chibotaru, L. F.; Leng, J.-D.; Guo, F.-S.; Tong, M.-L. The First {Dy4} Single-Molecule Magnet with a Toroidal Magnetic Moment in the Ground State. *Inorg. Chem.* **2012**, *51*, 1233.

(10) (a) Zhao, L.; Niel, V.; Thompson, L. K.; Xu, Z.; Milway, V. A.; Harvey, R. G.; Miller, D. O.; Wilson, C.; Leech, M.; Howard, J. A. K.; Heath, S. L. Self-assembled polynuclear clusters derived from some flexible polydentate dihydrazide ligands. *Dalton Trans.* **2004**, 1446−1455. (b) Abedin, T. S. M.; Thompson, L. K.; Miller, D. O. An octanuclear [Co(II)2−Co(III)2]2 interlocked grid—example of an inorganic [2]catenane. *Chem. Commun.* **2005**, 5512−5514.

(11) Sheldrick, G. M. Crystal structure refinement with SHELXL. G. M. Sheldrick. *Acta Crystallogr., Sect. A: Found. Adv.* **2015**, *71* (1), 3−8.

(12) Spek, A. L. PLATON SQUEEZE: a tool for the calculation of the disordered solvent contribution to the calculated structure factors. *Acta Crystallogr., Sect. C: Struct. Chem.* **2015**, *C71*, 1−2.

(13) Aquilante, F.; Autschbach, J.; Carlson, R. K.; Chibotaru, L. F.; Delcey, M. G.; De Vico, L.; Fdez. Galván, I.; Ferré, N.; Frutos, L. M.; Gagliardi, L.; Garavelli, M.; Giussani, A.; Hoyer, C. E.; Li Manni, G.; Lischka, H.; Ma, D.; Malmqvist, P. Å.; Müller, T.; Nenov, A.; Olivucci, M.; Pedersen, T. B.; Peng, D.; Plasser, F.; Pritchard, B.; Reiher, M.; Rivalta, I.; Schapiro, I.; Segarra-Martí, J.; Stenrup, M.; Truhlar, D. G.; Ungur, L.; Valentini, A.; Vancoillie, S.; Veryazov, V.; Vysotskiy, V. P.; Weingart, O.; Zapata, F.; Lindh, R. Molcas 8: New capabilities for multiconfigurational quantum chemical calculations across the periodic table. *J. Comput. Chem.* **2016**, *37*, 506−541.

(14) Ma, D.; Li Manni, G.; Gagliardi, L. The generalized active space concept in multiconfigurational self-consistent field methods. *J. Chem. Phys.* **2011**, *135*, 044128.

(15) (a) Hess, B. A.; Marian, C. M.; Wahlgren, U.; Gropen, O. A mean-field spin-orbit method applicable to correlated wavefunctions.

DOI: 10.1021/acs.inorgchem.6b02449
Inorg. Chem. XXXX, XXX, XXX−XXX

Chem. Phys. Lett. **1996**, *251*, 365−371. (b) Schimmelpfennig, B. *AMFI,* an atomic mean-field spin-orbit integral program; Stockholm University, 1996.
(16) (a) Douglas, M.; Kroll, N. M. Quantum electrodynamical corrections to the fine structure of helium. *Ann. Phys.* **1974**, *82*, 89−155. (b) Hess, B. A. *Phys. Rev. A: At., Mol., Opt. Phys.* **1986**, *33*, 3742−3748.
(17) Roos, B. O.; Lindh, R.; Malmqvist, P.-Å.; Veryazov, V.; Widmark, P.-O.; Borin, A. C. New Relativistic Atomic Natural Orbital Basis Sets for Lanthanide Atoms with Applications to the Ce Diatom and LuF3. *J. Phys. Chem. A* **2008**, *112*, 11431−11435.
(18) (a) Chibotaru, L. F.; Ungur, L. Ab initio calculation of anisotropic magnetic properties of complexes. I. Unique definition of pseudospin Hamiltonians and their derivation. *J. Chem. Phys.* **2012**, *137*, 064112. (b) Ungur, L.; Thewissen, M.; Costes, J.-P.; Wernsdorfer, W.; Chibotaru, L. F. Interplay of Strongly Anisotropic Metal Ions in Magnetic Blocking of Complexes. *Inorg. Chem.* **2013**, *52*, 6328−6337.
(19) Chibotaru, L. F.; Ungur, L.; Aronica, C.; Elmoll, H.; Pilet, G.; Luneau, D. Structure, Magnetism, and Theoretical Study of a Mixed-Valence CoII3CoIII4 Heptanuclear Wheel: Lack of SMM Behavior despite Negative Magnetic Anisotropy. *J. Am. Chem. Soc.* **2008**, *130*, 12445−12455.
(20) Neese, F. The ORCA program system. *WIREs Comput. Mol. Sci.* **2012**, *2*, 73−78.
(21) (a) Lee, C.; Yang, W.; Parr, R. G. Development of the Colle-Salvetti correlation-energy formula into a functional of the electron density. *Phys. Rev. B: Condens. Matter Mater. Phys.* **1988**, *37*, 785−789. (b) Becke, A. D. A new mixing of Hartree−Fock and local density-functional theories. *J. Chem. Phys.* **1993**, *98*, 1372−1377. (c) Becke, A. D. Density-functional thermochemistry. III. The role of exact Exchange. *J. Chem. Phys.* **1993**, *98*, 5648−5652. (d) Stephens, P. J.; Devlin, F. J.; Chabalowski, C. F.; Frisch, M. J. Ab Initio Calculation of Vibrational Absorption and Circular Dichroism Spectra Using Density Functional Force Fields. *J. Phys. Chem.* **1994**, *98*, 11623−11627.
(22) (a) Ruiz, E.; Cano, J.; Alvarez, S.; Alemany, P. Broken symmetry approach to calculation of exchange coupling constants for homobinuclear and heterobinuclear transition metal complexes. *J. Comput. Chem.* **1999**, *20*, 1391−1400. (b) Ruiz, E.; Rodríguez-Fortea, A.; Cano, J.; Alvarez, S.; Alemany, P. About the calculation of exchange coupling constants in polynuclear transition metal complexes. *J. Comput. Chem.* **2003**, *24*, 982−989.
(23) Lenthe, E. v.; Baerends, E. J.; Snijders, J. G. Relativistic regular two-component Hamiltonians. *J. Chem. Phys.* **1993**, *99*, 4597−4610.
(24) van Wüllen, C. Molecular density functional calculations in the regular relativistic approximation: Method, application to coinage metal diatomics, hydrides, fluorides and chlorides, and comparison with first-order relativistic calculations. *J. Chem. Phys.* **1998**, *109*, 392−399.
(25) Pantazis, D. A.; Chen, X.-Y.; Landis, C. R.; Neese, F. All-Electron Scalar Relativistic Basis Sets for Third-Row Transition Metal Atoms. *J. Chem. Theory Comput.* **2008**, *4*, 908−919.
(26) (a) Neese, F.; Wennmohs, F.; Hansen, A.; Becker, U. Efficient, approximate and parallel Hartree−Fock and hybrid DFT calculations. A 'chain-of-spheres' algorithm for the Hartree−Fock Exchange. *Chem. Phys.* **2009**, *356*, 98−109. (b) Izsak, R.; Neese, F. An overlap fitted chain of spheres exchange method. *J. Chem. Phys.* **2011**, *135*, 144105.
(27) Ruiz-Martínez, A.; Casanova, D.; Alvarez, S. Polyhedral Structures with an Odd Number of Vertices: Nine-Coordinate Metal Compounds. *Chem. - Eur. J.* **2008**, *14*, 1291−1303.
(28) (a) Bartolomé, J.; FIloti, G.; Kuncser, V.; Schinteie, G.; Mereacre, V.; Anson, C. E.; Powell, A. K.; Prodius, D.; Turta, C. Magnetostructural correlations in the tetranuclear series of {Fe3LnO2} butterfly core clusters: Magnetic and Mössbauer spectroscopic study. *Phys. Rev. B: Condens. Matter Mater. Phys.* **2009**, *80*, 014430. (b) Ishikawa, R.; Miyamoto, R.; Nojiri, H.; Breedlove, B. K.; Yamashita, M. Slow Relaxation of the Magnetization of an MnIII Single Ion. *Inorg. Chem.* **2013**, *52*, 8300.
(29) Gomez-Coca, S.; Aravena, D.; Morales, R.; Ruiz, E. Large magnetic anisotropy in mononuclear metal complexes. *Coord. Chem. Rev.* **2015**, *289*, 379.

DOI: 10.1021/acs.inorgchem.6b02449
Inorg. Chem. XXXX, XXX, XXX−XXX